ELSEVIER

Spectrochimica Acta Part B 55 (2000) 263–278

SPECTROCHIMICA ACTA PART B

www.elsevier.nl/locate/sab

Description of the argon-excited levels in a radio-frequency and direct current glow discharge

Annemie Bogaerts*, Renaat Gijbels

Department of Chemistry, Uni ersity of Antwerp (UIA), Uni ersiteitsplein 1, B-2610 Wilrijk-Antwerp, Belgium

Received 27 September 1999; accepted 17 December 1999

Abstract

A model to calculate the behavior of the excited argon levels, including the metastable levels, is developed for a glow discharge and applied to both the direct current and radio-frequency mode. Typical results are the level populations of these levels, as well as the relative contributions of different production and loss mechanisms. Moreover, the level populations, combined with the Einstein transition probabilities for radiative decay, allow us to calculate optical emission intensities. These results will be presented for both operation modes, and a comparison will be made. © 2000 Elsevier Science B.V. All rights reserved.

Keywords: Glow discharge; Direct current; Radio-frequency; Argon; Modeling; Collisional–radiative model; Metastable levels; Optical emission spectrometry

1. Introduction

Radio-frequency (rf) discharges are gaining increasing interest in analytical glow discharge spectrometry, mainly because they allow the direct analysis of non-conducting materials, and therefore, they widen the application field of glow discharge mass and optical emission spectrometry to a range of sample types. To understand better the differences between direct current (dc) and rf discharges, we try to describe the glow discharge by numerical models. In previous papers (e.g. [1–9]) we have developed a comprehensive modeling network for various species present in a dc glow discharge in argon with copper cathode: electrons, argon ions (Ar^+, Ar_2^+, Ar^{2+}), fast argon atoms, argon atoms in various excited levels, sputtered copper atoms and the corresponding ions, both in the ground state and in various excited

* Corresponding author. Tel.: 32-3-820-2364; fax: 32-3-820-2376.
E-mail address: bogaerts@uia.ua.ac.be (A. Bogaerts)

0584-8547/00/$ - see front matter
PII: S0584-8547(00)00143-9

levels (Cu^0, Cu*, Cu , Cu *). A similar model network has now been constructed for an rf discharge. The models describing the behavior of the electrons, Ar ions and fast argon atoms have been explained in some recent papers 10,11 , and for these species a comparison between the dc and rf mode has been made 12 . In the present paper, the model describing the argon atoms in various excited levels is presented. And to complete the modeling network, the model describing the sputtered copper atoms and ions will be reported in a subsequent paper 13 .

2. Description of the model

As mentioned before, the species assumed to be present in the plasma include electrons, argon (Ar , Ar_2 and Ar^2) ions, fast argon atoms, argon atoms in various excited levels, sputtered copper atoms and ions, also in the ground state and in excited levels. These species are described with a combination of Monte Carlo models (for the electrons, for the Ar ions, fast argon atoms and copper ions in the sheath adjacent to the cathode or rf-electrode, and for the thermalization of the copper atoms), fluid models (for the slow electrons and argon ions) and collisional–radiative models (for the excited argon and copper levels). These models are coupled to each other due to the interaction processes between the species. More information about these models can be found in Bogaerts et al. 1–9 ; only the collisional–radiative model describing the argon excited levels will be explained in more detail here.

The model describes the behavior of 64 excited levels. Some of these levels are individual levels (e.g. the four 4s metastable and resonant levels), but most of them are 'effective levels', i.e. a group of individual levels with similar excitation energy and quantum numbers. Fig. 1 shows the energy level scheme 7 , which was adopted from the model in Vlcek 14 . A subdivision is made depending on the ionization limit: the 'primed' system (j_c 1 2, corresponding to the ionization limit $^2P_{1\ 2}$ in Ar) and the 'unprimed' system (j_c 3 2, with ionization limit $^2P_{3\ 2}$ in Ar). The numbers in the squares indicate the effective level numbers of the excited levels. For a more detailed designation of all the excited levels, we refer to Bogaerts et al. 7 .

The populating and depopulating processes taken into account for these levels, are the following:

1. electron, fast argon ion, fast and thermal argon atom impact excitation and de-excitation between all the levels;
2. electron, fast argon ion, fast and thermal argon atom impact ionization from all the levels;
3. three-body electron–ion recombination to all levels, where the third body is an electron, fast argon ion, fast or thermal argon atom;
4. radiative electron–ion recombination to all levels;
5. radiative decay between all levels; and
6. Hornbeck–Molnar associative ionization for the levels with excitation energy above 14.71 eV (which is the ionization energy of Ar_2), i.e. Ar* $Ar^0 \rightarrow Ar_2$ e .

The four 4s levels play a key role in analytical glow discharges (e.g. for Penning ionization of the sputtered atoms), and they cannot easily be depopulated by radiative decay (due to forbidden transitions for the metastable levels, and due to radiation trapping for the resonant levels, see below). Therefore, some additional loss processes are incorporated for these levels, in order to describe them with more accuracy:

7. Penning ionization of the sputtered copper atoms;
8. 4s–4s collisions leading to the ionization of one of the atoms; or leading to the formation of Ar_2 (associative ionization);
9. two-body collisions with argon ground state atoms, yielding 'collision induced emission': Ar*(4s) $Ar^0 \rightarrow Ar^0$ Ar^0 $h\nu$;
10. three-body collisions with argon ground state atoms, leading to the formation of Ar_2^*: Ar*(4s) Ar^0 $Ar^0 \rightarrow Ar_2^*$ Ar^0; and
11. diffusion and subsequent de-excitation at the cell walls.

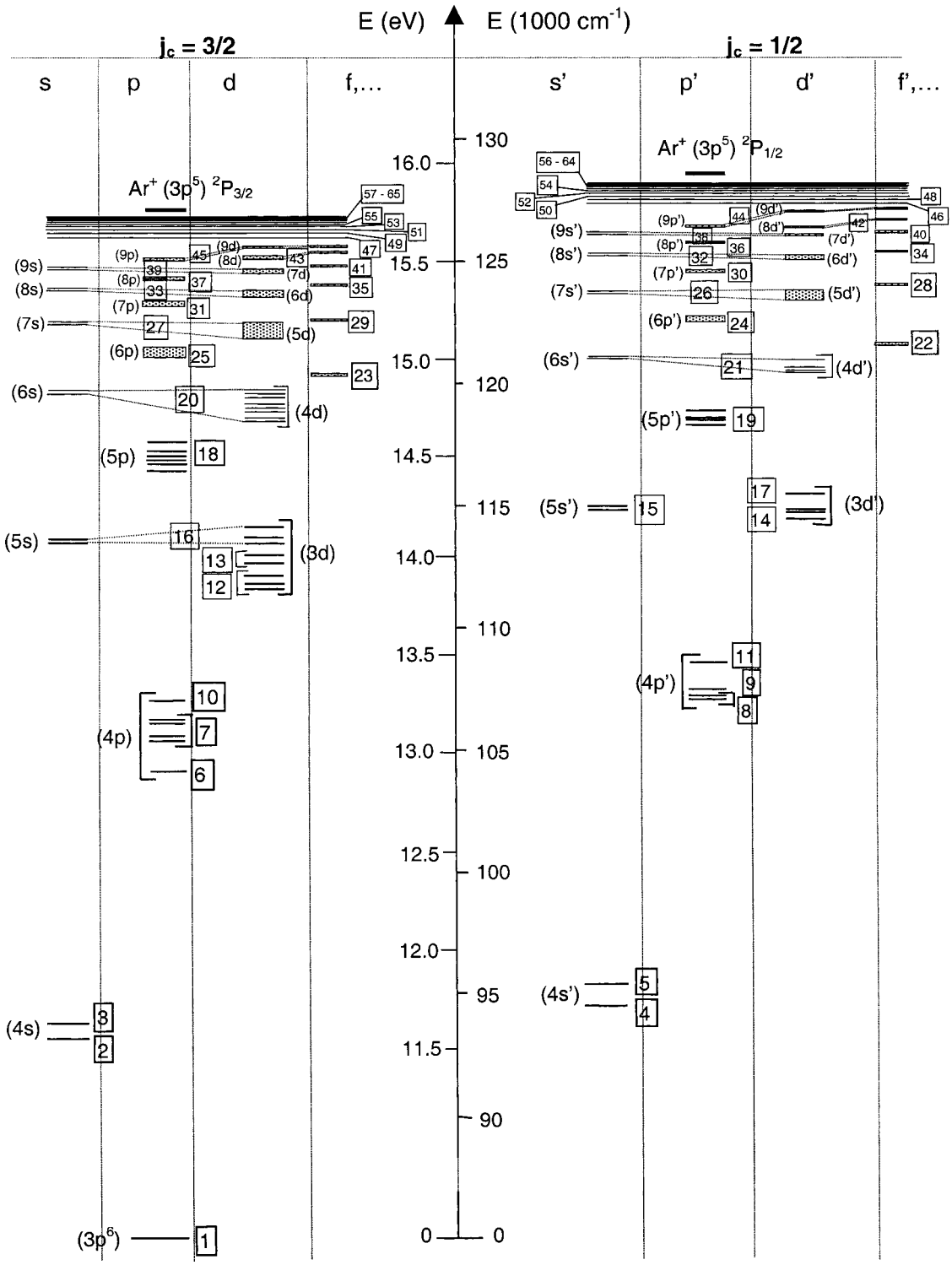

Fig. 1. Energy level scheme of the argon atom excited levels. Reprinted from Bogaerts et al. 7 with permission of the American Institute of Physics.

Finally, it should be mentioned that the radiative decay to the ground state is affected by so-called 'radiation trapping'. Indeed, the ground state argon atoms will reabsorb a fraction of the emitted radiation, so that only a small fraction (defined by the 'escape factor', in the order of 10^{-4} for pressures of approx. 1 torr) can really escape. Therefore, in calculating the radiative decay rate, the Einstein transition probability for radiative decay has to be multiplied with this escape factor, to yield the net decay rate. Because all these processes are either collisional or radiative, this kind of model is called a 'collisional–radiative' model.

The level populations of the 64 excited levels (i 2–65) are calculated with a set of 64 coupled balance equations, describing all the above mentioned populating and depopulating processes:

$$\frac{\partial n_i(z,r)}{\partial t} \quad \overline{\nabla}\cdot\overline{J}_i(z,r) \quad R_{\mathrm{pop},i}(z,r) \quad R_{\mathrm{depop},i}(z,r)$$

where n_i and J_i are the densities and fluxes of all levels i, and $R_{\mathrm{pop},i}$ and $R_{\mathrm{depop},i}$ comprise all populating and depopulating processes of level i (see above), all as a function of axial (z) and radial (r) direction (assuming that the glow discharge cell under study has cylindrical symmetry).

Transport of the levels occurs by diffusion, but it is only important for the 4s levels. Indeed, for the higher excited levels it can be neglected with respect to the collisional and radiative processes, as mentioned above:

$$\overline{J}_i(z,r) \qquad D\overline{\nabla}n_i(z,r)$$

where D is the diffusion coefficient, and the other symbols have been explained above.

Since the population of level i is determined by the higher and lower levels due to excitation, de-excitation, radiative decay, etc., the 64 balance equations for the 64 effective excited levels (i 2–65) are solved simultaneously, until convergence is reached. No balance equation is formulated for the argon ground state (i 1). Its density is simply calculated from the ideal gas law (n p kT) and is assumed to be uniform throughout the entire discharge.

All the cross sections, rate coefficients, transition probabilities, etc., were presented in Bogaerts et al. 7 and will therefore not be repeated here. The other data needed to calculate the production and loss rates, like densities, fluxes and energies of electrons, argon ions and atoms, are taken from the results of the models describing these plasma species. In this way, the present collisional–radiative model is coupled to the other models, and solved iteratively until convergence is achieved.

3. Results and discussion

3.1. Cell geometry and discharge conditions

The glow discharge cell under study is a Grimm-type cell with 4 mm anode diameter in the first few cm adjacent to the sample and 1.6 cm further away from the sample. The total length of the cell is approximately 8 cm. However, we found that the plasma was most intense in the first 1 cm from the cathode, and that most plasma processes were confined to this region 15 . Therefore, we have simplified the cell geometry, by assuming a simple cylinder with length 2 cm and diameter 4 mm. The cathode is found at one end of the cylinder whereas the other end of the cylinder as well as the side walls are at anode potential.

The discharge conditions under study are 5 torr gas pressure and 1100 K gas temperature, for both the rf and dc mode. For the dc discharge, a discharge voltage of 1000 V was assumed, from which an electrical current of 38.5 mA was calculated, and hence a discharge power of 38.5 W. For the rf discharge, the electrical power was used as input. A value of 37 W was assumed, yielding an rf voltage (rf amplitude) of 769 V and a dc bias voltage of 519 V. These values are in reasonable agreement with experimental values measured by Hoffmann 16 . Indeed, in a Grimm-type source with 4-mm anode diameter, he measured at a gas pressure of approximately 5 torr (and gas temperature unknown):

- for the dc discharge, V 1000 V and I 38 mA; and
- for the rf discharge, P 37 W, $V_{\text{rf-amplitude}}$ 680 V and $V_{\text{dc-bias}}$ 569 V.

Hence, the dc calculation results are in excellent agreement with experiment. The rf calculations, on the other hand, predicted a somewhat too high rf amplitude and a somewhat too low dc bias voltage. Nevertheless, the calculated values are in the correct order of magnitude, and what is more important, the comparison between rf and dc mode predicts the correct behavior (i.e. the rf mode requires lower voltages than the dc mode, for the same electrical power, due to more efficient ionization). This correct prediction is not straightforward, because in an earlier version of our rf model, the opposite trend was obtained (see also the discussion in Bogaerts et al. 12).

Fig. 2a illustrates the calculated and measured voltages in the rf-discharge as a function of time in one rf-cycle, as well as the dc bias in the rf-discharge (and the experimental value). Also the voltage in the dc discharge is depicted (which is given as input in the dc model and could therefore be taken equal to the experimental value). The calculated rf-amplitude is indeed slightly too high compared to the experimental data, and the dc bias is somewhat lower than the measured value, but the general trend is very similar.

The calculated rf electrical current, as a function of time in the rf-cycle, is presented in Fig. 2b, together with the contributions of electron and ion currents bombarding the rf-electrode and the displacement current (i.e. the current as a result of the moving of the rf-sheath; see 10 for more explanation). The latter current plays only a minor role for the discharge conditions under study here, because the sheath does not vary significantly in thickness, in contrast to low-pressure discharges (mtorr range). During most of the rf-cycle, the current is predominantly carried by ions bombarding the rf-electrode; only at ωt π 2, when the rf-electrode has a positive potential (see Fig. 2a), the electrical current is determined to a large extent by the electrons bombarding the rf-electrode. The total electrical current, integrated over the entire rf-cycle, is zero, which is imposed by the capacitive rf-coupling. For comparison, also the calculated total dc current is plotted in Fig. 2b (constant in time). It is slightly lower than the rf current during most of the rf-cycle, and clearly lower (but with opposite sign) at ωt π 2. This is like expected because the dc voltage is higher than in the rf case (see above), and the power levels are similar.

Finally, in Fig. 2c the calculated electrical power as a function of time in the rf-cycle is depicted. The time-averaged value is also indicated, as well as the calculated dc value. Both values are nearly

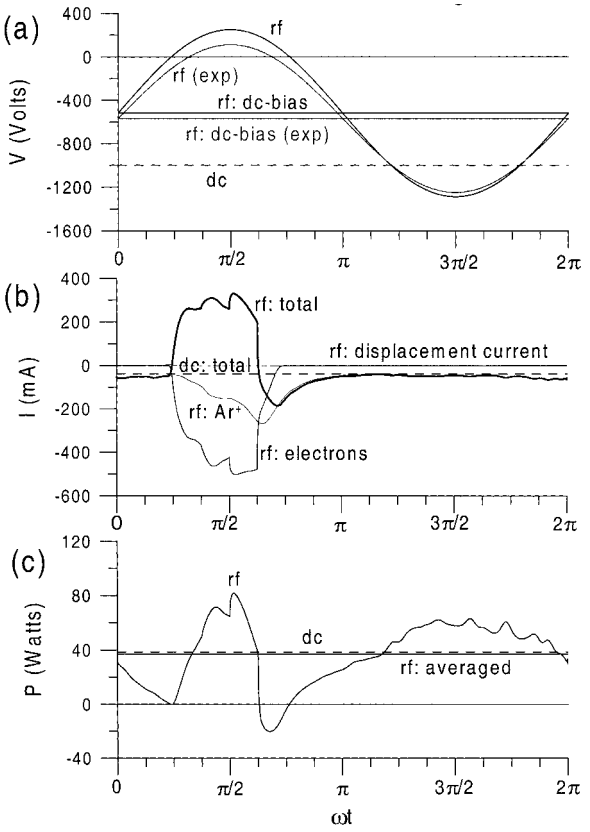

Fig. 2. Calculated electrical characteristics of the glow discharges under study, both in the rf mode (solid lines; as a function of time in the rf cycle) and in the dc mode (dashed lines): (a) voltage (the measured values are also shown, in gray lines), (b) current, including the contributions of ion and electron current at the rf-electrode and displacement current (in the rf case), and (c) electrical power.

equal to each other. This was indeed our intention, because it makes comparison of other calculated quantities more meaningful.

3.2. Le el populations of the argon excited le els

Fig. 3 shows the two-dimensional density profiles of the four 4s levels in the rf-discharge, which are constant throughout the entire rf-cycle. The rf-electrode is found at the left end of the figure. Levels i 2 and 4 are the metastable levels whereas levels i 3 and 5 are the resonant levels. All four levels reach a maximum density very close to the rf-electrode; then the density drops but it reaches a second maximum at approximately 1.5 cm from the rf-electrode. Looking at the absolute values, level i 2 is slightly higher than levels i 3 and 4, which are in turn slightly higher than level i 5. This corresponds well to our previous results for a dc discharge at other conditions 7 , and is also generally in good agreement with data from the literature 17,18 . The pronounced maximum near the rf-electrode is due to electron, but also argon ion and fast argon atom impact excitation of the levels from the ground state, whereas the second maximum is entirely due to electron impact excitation. Indeed, the electric field in the bulk plasma can take considerably high values at ωt π 2, because the high potential at the rf-electrode around this time (see Fig. 2a) needs to fall off till zero at the grounded cell walls. This high electric field (and the large potential drop) in the bulk plasma were presented in Bogaerts et al. 10,12 . As a result of this electric field in the bulk plasma, the electrons are characterized here by considerable energies, which allow them to give rise to ionization and excitation collisions. The rather large amount of ionization in the bulk plasma at ωt π 2 (see Bogaerts et al. 10,12), on one hand, is responsible for the lower voltages in the rf mode compared to the dc mode. The considerable amount of excitation, on the other hand, results in rather high densities of the excited atoms in the bulk plasma, as is shown in Fig. 3. Indeed, when we compare these rf density profiles with the dc two-dimensional density profiles, presented in Fig. 4, it appears that this second maximum in the level profiles has clearly dropped (for levels i 2 and 4) or has even completely disappeared (for levels i 3 and 5) in the dc case. Beside this, the dc density profiles strongly resemble the rf density profiles, with a pronounced maximum close to the cathode and very similar absolute values.

Similar features are observed for the other excited argon levels. Fig. 5 presents an overview of some representative levels: the 4p 1 2_1 level, i.e. the lowest 4p level (i 6) in Fig. 5a; the 4p 1 2_0 level, i.e. one of the highest 4p levels (i 10) in Fig. 5b; a group of 3d levels (i 12) in Fig. 5c; the 5p levels (i 18) in Fig. 5d; the 6p levels (i 25) in Fig. 5e; and one of the higher effective levels (i 40) in Fig. 5f. In each case the one-dimensional density profiles are shown for the rf discharge at four times in the rf-cycle (black curves) and for the dc discharge (gray line). It is clear that the density of all these levels reaches its maximum rather close to the rf-electrode (or cathode), i.e. at the boundary between rf-sheath and bulk plasma, due to electron impact excitation. For the 4p levels (Fig. 5a,b) a small peak is also observed adjacent to the electrode, due to fast argon ion and atom impact excitation, but this peak is absent for the higher levels, because they require too much energy for excitation, and the ions and atoms do not have such high energies. Further in the discharge, the dc density profiles drop considerably, because the electrons are not able to excite the levels anymore. In the rf discharge, the density profiles are characterized by still rather high values in the bulk plasma, because the electrons can still give rise to excitation (see above). However, the degree of excitation in the bulk plasma appears to be slightly time-dependent. At ωt π 2, when the electric field in the bulk plasma is considerable, the excitation by electrons in the bulk plasma, and hence the excited level populations, are rather high. At later times in the rf-cycle, the bulk electric field is rather low and the electron energy drops gradually, giving rise to gradually less excitation, and hence lower level populations, in the bulk plasma. This behavior appears to be similar for all excited levels. However, for the highly excited levels (e.g. i 40) the density decreases more rapidly at distances further away

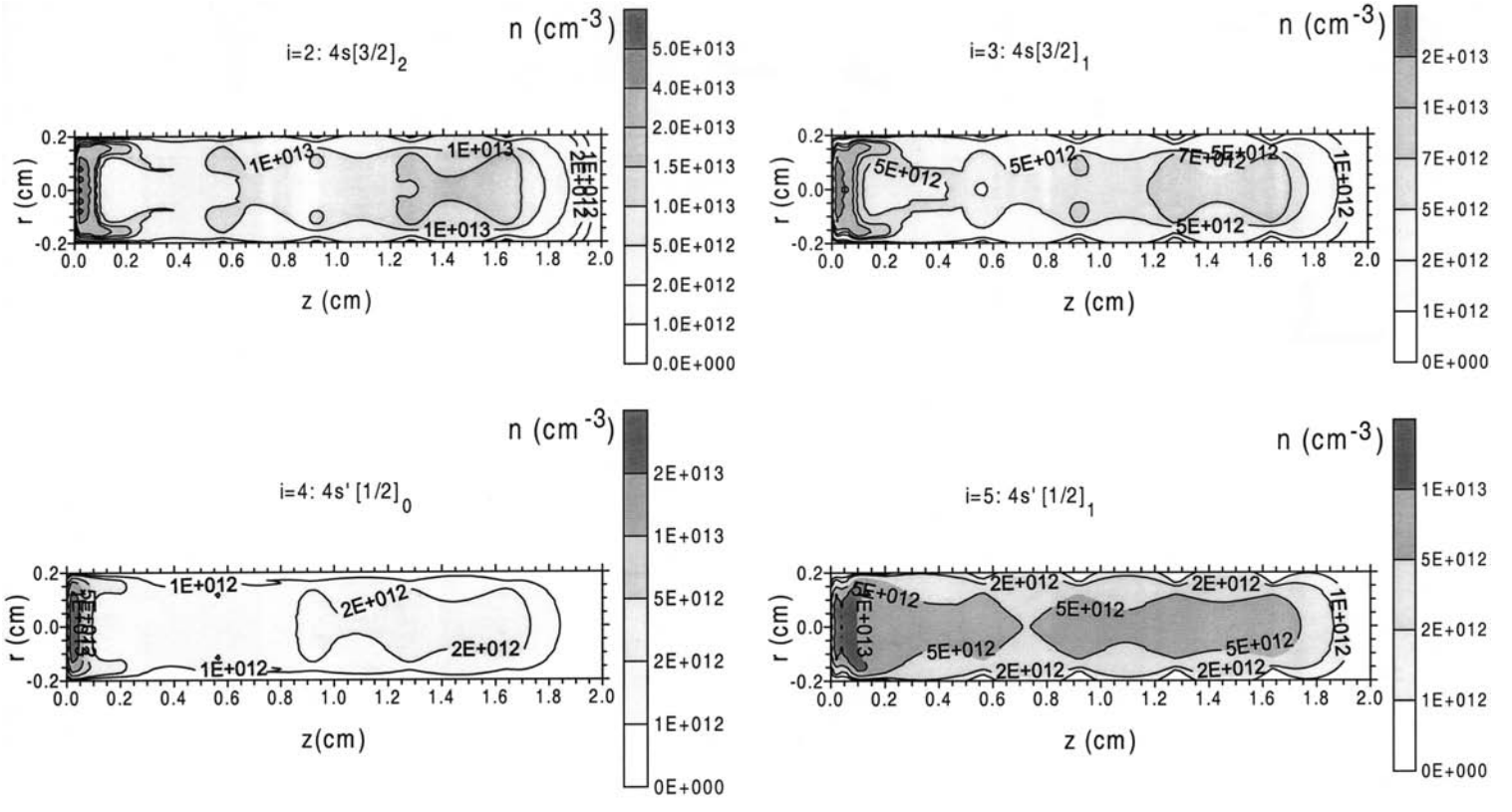

Fig. 3. Calculated two-dimensional density profiles of the four 4s levels in the rf discharge (at 5 torr, 37 W, 769 V rf amplitude and 519 V dc bias).

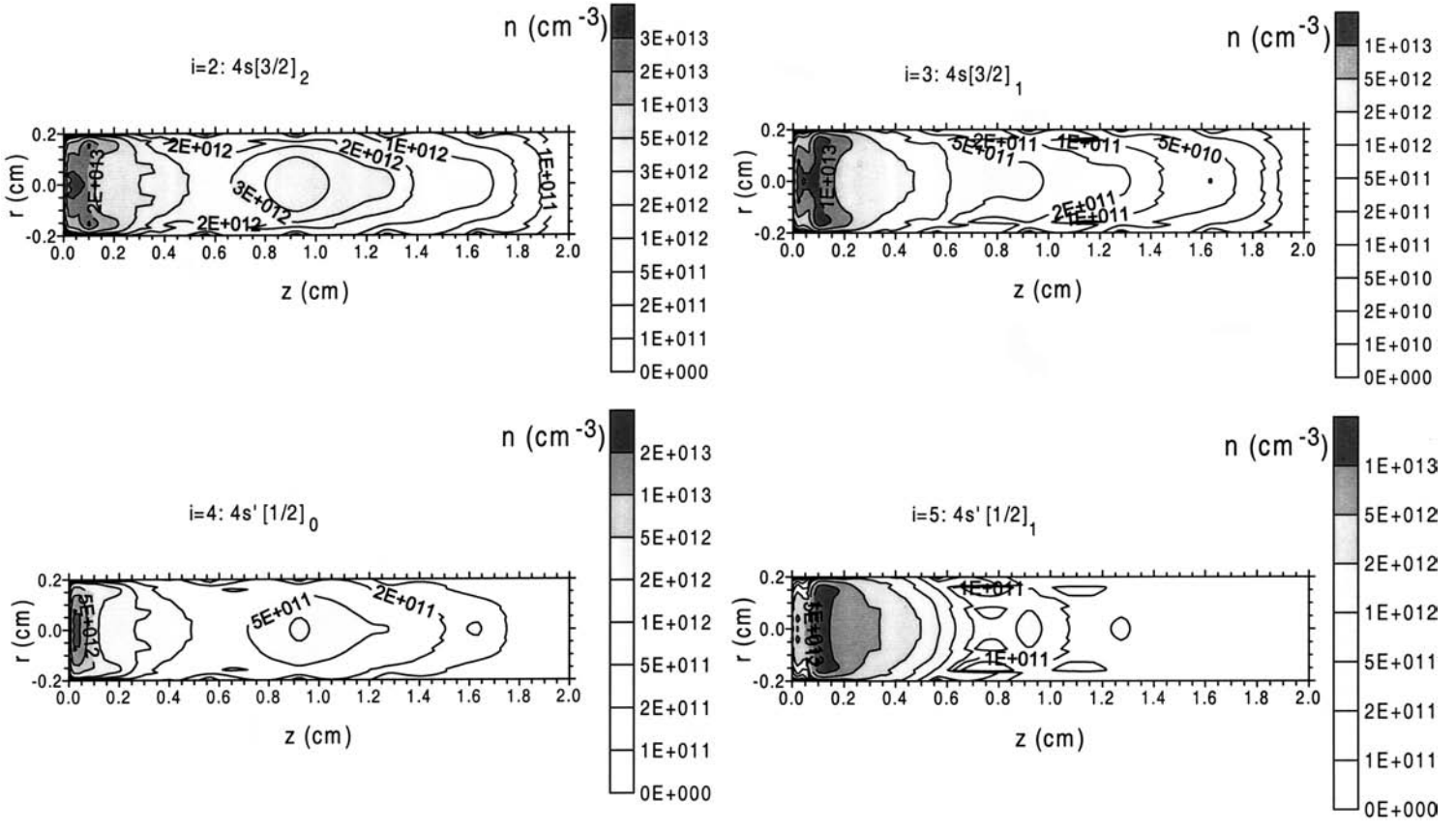

Fig. 4. Calculated two-dimensional density profiles of the four 4s levels in the dc discharge (at 5 torr, 38.5 W, 1000 V).

from the electrode, because the electrons in the bulk plasma have not enough energy to excite these high levels. Moreover, the level populations of these high energy levels appear to be much lower, at their maximum, in the dc discharge than in the rf discharge (see Fig. 5f).

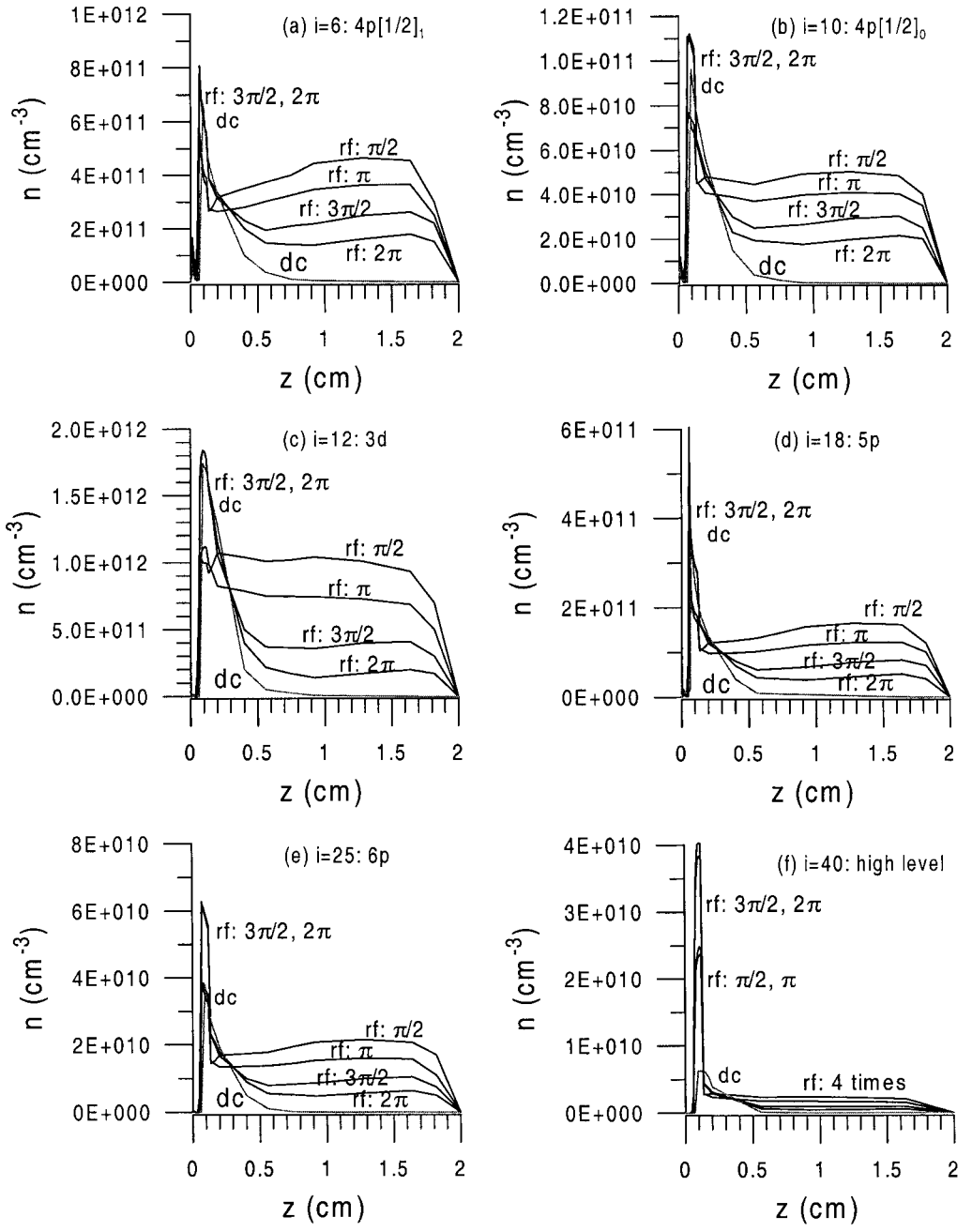

Fig. 5. Calculated one-dimensional density profiles of some higher excited levels in the rf discharge (at four times in the rf cycle) and in the dc discharge, for the same conditions as in Figs. 3 and 4. (a) i 6 (lowest 4p level: 4p 1 2_1); (b) i 10 (high 4p level: 4p 1 2_0); (c) i 12 (group of 3d levels); (d) i 18 (5p levels); (e) i 25 (6p levels); and (f) i 40 (as a representative for the higher levels).

The latter is also observed very clearly in Fig. 6. Indeed, this figure shows the level populations at the maximum of their profiles against the level number i, both for the rf discharge at four times in the rf-cycle (black lines, full circles) and for the dc discharge (gray lines, squares). The dashed line with triangles represents the statistical weights of the levels (right axis). For the excited levels up to level number $i \sim 25$ (i.e. the 6p levels), the level populations appear to be very similar for both operation modes. However, for the higher excited levels, the dc mode yields systematically lower densities, and this behavior becomes very pronounced for level numbers higher than approximately i 40–45, probably due to less efficient excitation to these high levels in the dc case. Moreover, it appears from Fig. 6 that, especially for the higher levels, there are some variations of the level populations as a function of time; however, this effect is only of minor importance. Finally, it should be mentioned that the level populations of the uneven level numbers (i.e. the unprimed system) are systematically higher than the corresponding level populations of the primed system, both in the dc and the rf mode. The main reason for this is simply the higher statistical weights of the levels in the unprimed system (see the dashed line). The increasing statistical weight of the higher excited effective levels also explains why the level populations do not really drop with rising excitation energy, as would be expected.

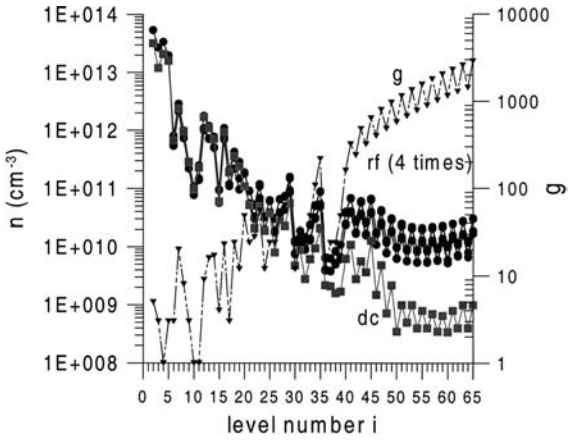

Fig. 6. Calculated level populations at the maximum of their profiles, for all excited levels, in the rf-discharge (at four times in the rf cycle) and in the dc discharge, at the same conditions as in Figs. 3 and 4. Also illustrated in the figure are the statistical weights of the excited levels.

3.3. Relati e contributions of the different populating and depopulating processes

Table 1 summarizes the relative contributions of the main processes populating or depopulating the excited levels, in the rf discharge at four times in the rf-cycle, and also in the dc discharge. Two 4s levels are presented (i 2 and 3, i.e. a metastable and a resonant level), as well as a low and a high 4p level (i 6 and 10), a group of 3d levels (i 12), a group of 5p levels (i 18) and level i 31, as a representative for the higher excited levels.

The 4s levels seem to be mainly populated by radiative decay from the 4p levels, as well as from electron impact excitation from the ground state and electron impact excitation or de-excitation from lower or higher 4s levels, respectively. The most important loss process seems to be electron impact excitation to higher levels, especially the 4p levels. Moreover, the resonant 4s levels (i 3 and 5) are also depopulated for approximately 10% by radiative decay to the ground state. Other processes, like electron impact ionization, 4s–4s collisions and Penning ionization contribute for a few percentages. These calculated relative contributions vary only slightly over time. Moreover, there are no pronounced differences between the dc and rf mode, except that electron impact excitation becomes slightly more, and radiative decay slightly less important as a production process in the dc mode. The reason is probably not that electron impact excitation is more efficient in the dc mode than in the rf-mode (because the calculated 4s level populations do not appear higher in the dc mode), but rather that radiative decay occurs less in the dc mode. Indeed, radiative decay can in principle occur in the entire discharge, because the transition probabilities are not dependent on position. Since the level populations in the dc discharge generally drop very fast to low values at distances further from the cathode, they can, however, only give rise to ra-

Table 1
Relative contributions (in%) of the most important populating and depopulating processes

Level	Processes	rf: π 2	rf: π	rf: 3π 2	rf: 2π	dc
i 2: 4s 3 2 $_2$	Populating processes:					
	Radiative decay from 4p	65.9	65.3	63.1	60.7	47.9
	Electron excitation from ground	19.2	17.9	18.3	17.4	28.5
	Electron de-excitation from higher 4s	11.6	13.8	15.3	17.9	17.4
	Electron de-excitation from 4p	2.0	1.9	2.2	2.3	3.5
	Fast Ar and Ar^0 impact excitation from ground	0.7	0.5	0.6	1.1	0.5
	Depopulating processes:					
	Electron impact excitation to higher 4s	15.1	15.9	16.6	17.9	15.9
	Electron impact excitation to 4p	58.2	57.9	57.4	56.5	58.5
	Electron impact excitation to higher levels	17.9	18.1	17.6	17.2	18.0
	Electron impact ionization	4.4	4.1	3.9	3.6	4.3
	Penning ionization of sputtered atoms	0.7	0.7	0.7	0.8	0.4
	4s–4s level collisions	3.4	3.4	3.7	3.8	1.4
i 3: 4s 3 2 $_1$	Populating processes:					
	Radiative decay from 4p	49.1	49.2	46.7	44.3	33.6
	Electron excitation from ground	28.8	25.1	25.7	23.6	39.3
	Electron excitation from lower 4s	16.7	20.1	21.7	24.8	19.4
	Electron de-excitation from higher 4s	2.1	2.5	2.7	3.2	3.6
	Electron de-excitation from 4p	1.6	2.0	1.8	1.9	2.7
	Fast Ar and Ar^0 impact excitation from ground	1.1	0.8	0.9	1.6	0.7
	Depopulating processes:					
	Electron impact excitation to higher 4s	2.3	2.4	2.5	2.6	2.5
	Electron impact de-excitation to lower 4s	18.2	19.0	19.5	20.7	20.6
	Electron impact excitation to 4p	48.4	47.8	46.6	46.0	52.0
	Electron impact excitation to higher levels	14.6	14.3	13.8	12.6	15.0
	Electron impact ionization	3.7	3.4	3.3	3.0	3.8
	Radiative decay to ground state	10.5	10.7	11.2	11.4	4.7
	Penning ionization of sputtered atoms	0.4	0.5	0.5	0.5	0.2
	4s–4s level collisions	1.9	1.9	2.0	2.0	0.8
i 6: 4p 1 2 $_1$	Populating processes:					
	Electron impact excitation from ground	23.7	21.0	21.9	20.9	29.0
	Electron impact excitation from 4s	30.0	35.6	37.3	40.9	31.2
	Electron impact de-excitation from higher levels	7.9	7.9	9.4	10.1	14.4
	Radiative decay from higher levels	37.7	34.9	30.9	27.4	25.1
	Fast Ar and Ar^0 impact excitation from ground	0.2	0.1	0.2	0.4	0.1
	Depopulating processes:					
	Radiative decay to 4s	54.4	53.4	48.7	46.0	30.6
	Electron impact excitation to 3d 5s 5p levels	33.1	33.5	37.2	39.2	50.5
	Electron impact excitation to higher levels	9.3	9.9	10.4	10.9	13.9
	Electron impact de-excitation to 4s	2.2	2.2	2.5	2.6	3.3
	Electron impact ionization	1.0	0.9	1.1	1.1	1.4
i 10: 4p 1 2 $_0$	Populating processes:					
	Electron impact excitation from ground	25.5	21.7	21.7	20.1	26.9
	Electron impact excitation from 4s	40.9	46.4	46.7	49.4	41.0
	Electron impact de-excitation from higher levels	13.8	13.4	15.2	15.9	20.7
	Radiative decay from higher levels	19.3	18.0	15.9	14.2	10.9
	Fast Ar and Ar^0 impact excitation from ground	0.1	0.1	0.1	0.2	0.1

Table 1 (*Continued*)

Level	Processes	rf: π 2	rf: π	rf: 3π 2	rf: 2π	dc
	Depopulating processes:					
	Radiative decay to 4s	55.2	54.5	50.7	48.0	35.2
	Electron impact excitation to 3d 5s 5p levels	27.4	28.1	31.2	33.7	44.6
	Electron impact excitation to higher levels	6.9	7.0	7.9	8.4	11.2
	Electron impact de-excitation to 4s	1.4	1.4	1.6	1.7	2.2
	Ar atom impact de-excitation to lower 4p	8.2	8.1	7.6	7.2	5.3
	Electron impact ionization	0.7	0.7	0.8	0.8	1.1
i 12: 3d	Populating processes:					
	Electron impact excitation from ground	79.9	77.1	75.9	74.0	79.1
	Electron impact excitation from 4s	6.5	8.2	8.3	9.1	5.5
	Electron impact excitation from 4p	10.3	11.2	12.1	13.1	12.3
	Electron impact de-excitation from higher levels	1.4	1.7	1.9	2.2	2.0
	Radiative decay from higher levels	0.9	0.9	0.9	0.8	0.5
	Depopulating processes:					
	Radiative decay to 4p	53.2	51.8	43.7	38.8	29.0
	Electron impact excitation to higher levels	27.6	28.5	33.2	36.5	41.0
	Electron impact de-excitation to 4p	14.0	14.6	16.9	18.4	20.8
	Electron impact de-excitation to 4s	0.4	0.5	0.5	0.6	2.9
	Electron impact ionization	4.4	4.3	5.2	5.6	6.2
i 18: 5p	Populating processes:					
	Electron impact excitation from ground	17.6	14.6	13.7	12.1	14.0
	Electron impact excitation from 4s	0.3	0.3	0.3	0.3	0.2
	Electron impact excitation from 4p	53.8	56.1	55.4	56.1	54.6
	Electron impact excitation from 3d 5s	17.4	17.7	18.5	18.9	19.8
	Electron impact de-excitation from higher levels	10.5	10.9	11.8	12.2	10.8
	Radiative decay from higher levels	0.3	0.3	0.2	0.2	0.1
	Depopulating processes:					
	Electron impact excitation to 4d 6s	18.1	18.0	18.2	18.2	18.4
	Electron impact excitation to 5d 7s	47.7	48.1	48.2	48.4	48.7
	Electron impact excitation to other higher levels	17.8	17.6	17.8	17.8	18.1
	Electron impact de-excitation to lower levels	12.5	12.5	12.6	12.6	12.7
	Radiative decay to lower levels	3.0	2.6	2.2	1.8	1.1
	Electron impact ionization	0.8	0.8	0.8	0.8	0.8
i 31: 7p	Populating processes:					
	Electron impact excitation from 4p	8.3	8.1	7.5	7.3	8.4
	Electron impact excitation from 5p	16.2	15.6	14.8	14.3	16.3
	Electron impact excitation from 6p	52.6	52.7	51.9	51.8	54.4
	Electron impact excitation from 5d 7s 5f,g	4.9	4.9	5.5	5.6	4.9
	Electron impact de-excitation from higher levels	17.7	18.3	19.9	20.4	15.9
	Depopulating processes					
	Hornbeck–Molnar associative ionization	94.6	95.2	96.4	96.3	89.3
	Electron impact excitation to higher levels	4.2	3.7	2.8	2.9	8.4
	Electron impact de-excitation to lower levels	1.2	1.0	0.8	0.8	2.3

diative decay in the first millimeters from the cathode. The level populations in the rf discharge, on the other hand, are still quite high in the bulk plasma and, therefore, they can decay radiatively over the whole discharge region, which increases the relative contribution of radiative decay as production and loss process in the rf mode. This explains also why radiative decay becomes slightly less important from $\omega t \quad \pi \ 2$ to $\omega t \quad 2\pi$, because the excited level populations in the bulk plasma are higher at $\omega t \quad \pi \ 2$ than at $\omega t \quad 2\pi$.

From Table 1 it follows further that the 4p levels ($i \quad 6$ and 10) are predominantly populated by stepwise electron impact excitation from the 4s levels, although direct excitation from the ground state still plays a significant role. Moreover, electron impact de-excitation and radiative decay from higher excited levels are also quite important production processes. Depopulation of the 4p levels occurs mainly by radiative decay to the 4s levels and by electron impact excitation to higher levels (especially the 3d, 5s and 5p levels). Again, the relative contributions of the populating and depopulating processes do not vary significantly in time, and are also quite similar for both the rf and dc mode. Again it appears that radiative decay occurs to a somewhat less extent, both as production and loss process, in the dc mode compared to the rf mode, and also within the rf mode at $\omega t \quad 2\pi$ compared to $\omega t \quad \pi \ 2$, for the reason given above.

The 3d levels ($i \quad 12$) appear to be mainly populated by electron impact excitation from the ground state, and to a somewhat less extent, from the 4s and 4p levels. The most important loss processes are electron impact excitation to the higher levels (especially for the dc mode) and radiative decay and electron impact de-excitation to the 4p levels. The variations as a function of time in the rf discharge, and between the rf and dc mode, i.e. a decreasing contribution of radiative decay as a loss process in the dc mode and at $\omega t \quad 2\pi$ compared to $\omega t \quad \pi \ 2$, is similar as described above.

The most significant production processes for the 5p levels ($i \quad 18$) are direct electron impact excitation from the ground state, and especially stepwise excitation from the 4p, 3d and 5s levels. Also electron impact de-excitation from higher levels plays a non-negligible role, but radiative decay from these higher levels becomes of minor importance for the population of these 5p levels. It is indeed a general trend, also observed before 7, that radiative decay becomes less important, both as production and loss process, for the higher excited levels. This becomes also obvious from the relative contributions of the loss processes for the 5p levels. Indeed, radiative decay appears to play only a minor role compared to electron impact excitation to higher levels (especially the 4d, 6s, 5d and 7s levels) and de-excitation to lower levels. Therefore, the variations in relative contributions as a function of time in the rf-cycle, as well as between the rf and dc mode, have now more or less disappeared.

Finally, the relative contributions of production and loss processes for the 7p levels ($i \quad 31$) are presented, as a representative of the higher levels. It appears that they are mainly populated by stepwise electron impact excitation from lower levels (i.e. especially the 6p and 5p levels) although de-excitation from higher levels also plays an important role. The loss for these higher levels (starting from the 4d and 6s levels) is primarily due to the Hornbeck–Molnar associative ionization, leading to the formation of Ar_2 ions.

3.4. Optical emission spectra

As mentioned before, from the level populations of the excited levels, multiplied with the Einstein transition probabilities for radiative decay, the optical emission intensities can be calculated. We have carried this out for 605 argon atom lines. In Fig. 7, the intensities of three emission lines are plotted as a function of distance from the electrode, both in the rf discharge at four times in the rf-cycle (black curves), and in the dc discharge (gray line), i.e. the 811.53 nm line (originating from a 4p level), the 434.52 nm line (corresponding to a 5p–4s transition) and the 549.75 nm line (representing a 6d–4p transition). As could be expected already from the one-dimensional density profiles, the maximum emis-

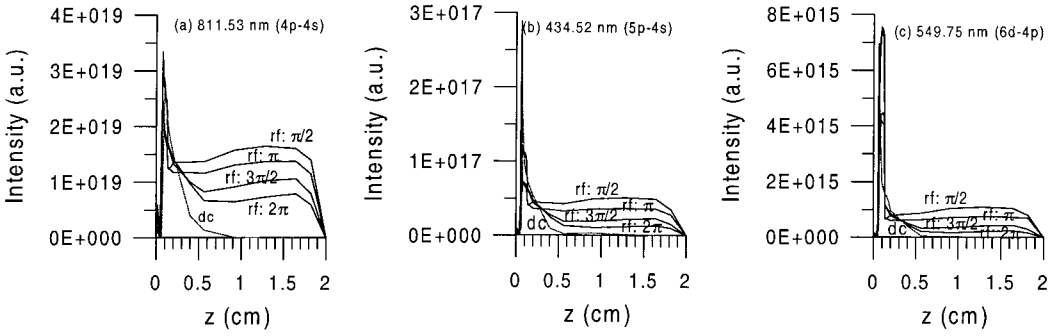

Fig. 7. Calculated emission intensities as a function of axial distance from the electrode, in the rf-discharge (at four times in the rf cycle) and in the dc discharge, at the same conditions as in Figs. 3 and 4. (a) λ 811.53 nm (corresponding to a 4p–4s transition; (b) λ 434.52 nm (representing a 5p–4s transition); and (c) λ 549.75 nm (6d–4p transition).

sion intensity is found rather close to the rf-electrode cathode, at the sheath–bulk plasma boundary, after which the intensity drops rather quickly in the dc case. In the rf case, however, the intensity is still rather high in the bulk plasma, due to the rather high excited level populations. This is especially true for the 811.53-nm line (4p–4s transition). The absolute values at the maximum of the profile are very similar for both the dc and rf discharge, although for the lines originating from higher levels (e.g. the 549.75-nm line), the dc values are systematically lower than the rf values. Hence, from the somewhat lower maximum values and the faster drop as a function of distance in the dc discharge, it is expected that the intensities integrated in the axial direction (which is observed in an end-on optical emission spectrum) will be somewhat lower in the dc case than in the rf case.

The latter is illustrated more clearly in Fig. 8, which shows the calculated optical emission spectra, like in end-on observation, for both the rf and the dc discharge. The rf spectrum was found to be identical at all times in the rf cycle investigated. This calculated spectrum has been checked against experiment in a previous paper [19] for the dc discharge, and satisfactory agreement has been reached.

The spectra are presented on a semi-logarithmic plot, in order to show the large number of lines. It follows that the region of 700–1000 nm is characterized by the most intense lines, i.e. the so-called 'red lines', corresponding to 4p–4s transitions. Furthermore, the region of 380–470 nm also contains rather strong lines, the so-called 'blue lines', corresponding to 5p–4s transitions. From comparing the rf and dc spectra, it becomes indeed obvious that the dc lines are somewhat less intense than the rf lines. The difference is, however, less than a factor of approximately 2, so that we can conclude that our model calculations predict, for the same power levels, similar argon optical emission spectra in the rf and dc modes. It is not clear whether this is also found experimentally, because the argon emission spectra are not routinely being measured by analytical spectroscopists. However, a similar behavior seems to be observed experimentally for the Cu emission intensities, which have been found to be slightly higher in the rf discharge compared to the dc discharge [16].

4. Conclusion

A collisional–radiative model, describing the behavior of 64 argon excited levels, has been developed and applied to argon glow discharges operated in both the dc and rf mode. The discharge conditions are typical for a Grimm-type glow discharge, i.e. 5 torr gas pressure, an electrical power of 37 W (rf) and 38.5 W (dc), a dc voltage of 1000 V, and rf voltages of 769 V (rf amplitude) and 519 V (dc bias). These calcu-

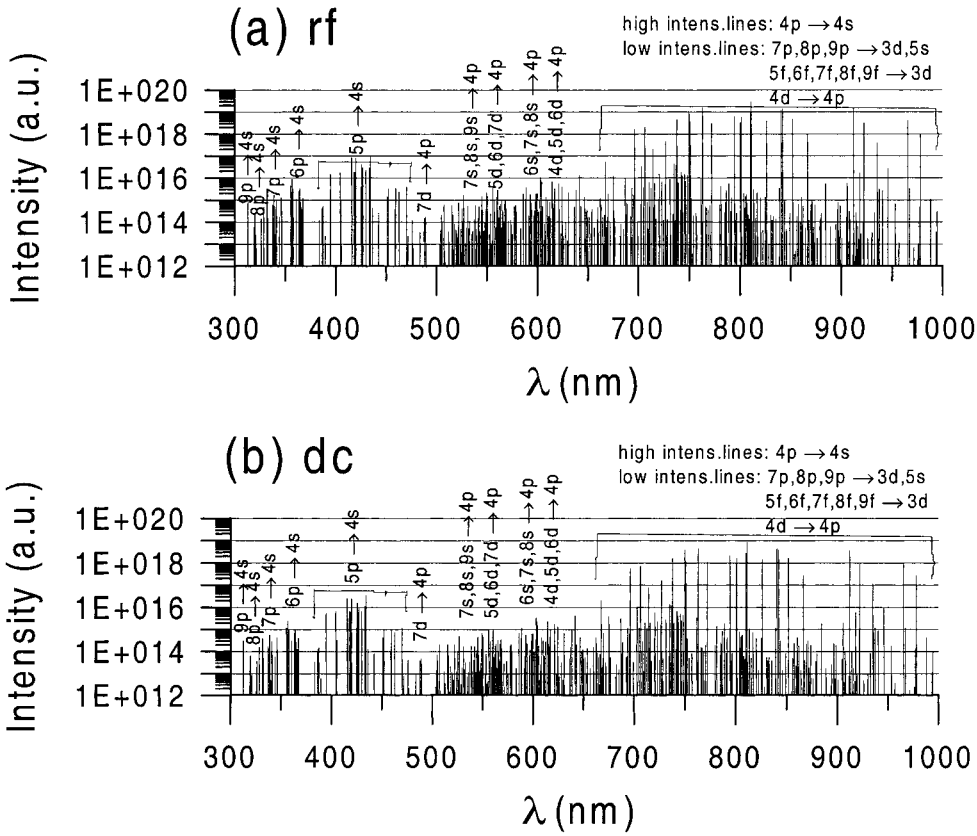

Fig. 8. Calculated 'end-on' optical emission spectra, (a) in the rf-discharge (similar at all times in the rf cycle) and (b) in the dc discharge, for the same conditions as in Figs. 3 and 4.

lated discharge conditions are in reasonable agreement with measurements performed by Hoffmann [16].

The level populations of all excited levels are found to reach a maximum close to the rf-electrode (or cathode), at the boundary between sheath and bulk plasma, as a result of electron impact excitation. The 4s levels and the low 4p levels are also formed by fast argon ion and atom impact ionization, which occur adjacent to the rf-electrode, but this peak overlaps more or less with the peak due to electron impact excitation. In the dc discharge, the level populations drop rather quickly in the bulk plasma. In the rf discharge, on the other hand, the populations are still considerable in the bulk plasma, due to electron impact excitation by electrons heated from the fluctuating electric field in the bulk plasma. The absolute values in both operation modes are very similar, although for the highly excited levels the absolute value decreases more rapidly for the dc discharge compared to the rf discharge.

Concerning the relative contributions of various populating and depopulating processes, we found that direct electron impact excitation from the ground state and stepwise excitation from lower excited levels are the most important production processes, as well as radiative decay and electron impact de-excitation from higher levels. Similarly, electron impact excitation to higher levels and de-excitation to lower levels are very important loss processes, together with radiative decay to lower levels. The latter process is, however, slightly less significant in the dc mode, and becomes in general also less important for the higher levels. These high energy levels, on the

other hand, starting from the 4d and 6s levels, are primarily depopulated by Hornbeck–Molnar associative ionization.

Finally, from the level populations of the excited levels, multiplied by the Einstein transition probabilities for radiative decay, the optical emission intensities could be calculated. The intensities of three optical emission lines are plotted as a function of distance from the electrode, for both the rf discharge (at four times in the rf-cycle) and for the dc discharge. The axial dependence is identical to the axial level population profiles. By integrating the line intensities over axial distance, the 'end-on observed' optical emission spectrum could be calculated. This calculated spectrum has been checked against experiment in a previous paper for the dc discharge. It contains a large number of lines (the intensities were calculated for 605 lines) but the so-called red lines (corresponding to 4p–4s transitions, between 700 and 1000 nm) are clearly dominant, followed by a group of blue lines between 380 and 470 nm (corresponding to 5p–4s transitions). The dc spectral intensities were calculated to be slightly lower than the corresponding rf intensities, but the general outlook of both spectra is very similar.

In a subsequent paper, the model describing the copper atomic and ionic excited levels will be explained, and typical results like copper excited level populations, sputtering rates and optical emission intensities, will be presented and compared between both operation modes.

Acknowledgements

A. Bogaerts is financed by the Flemish Fund for Scientific Research (FWO). This research is also sponsored by the Federal Services for Scientific, Technical and Cultural Affairs of the Prime Minister's Office through IUAP-IV (Conv. P4 10). Finally, we wish to thank V. Hoffmann for supplying us with the experimental data.

References

1 A. Bogaerts, M. van Straaten, R. Gijbels, Spectrochim. Acta Part B 50 (1995) 179.
2 A. Bogaerts, M. van Straaten, R. Gijbels, J. Appl. Phys. 77 (1995) 1868.
3 A. Bogaerts, R. Gijbels, W.J. Goedheer, J. Appl. Phys. 78 (1995) 2233.
4 A. Bogaerts, R. Gijbels, J. Appl. Phys. 79 (1996) 1279.
5 A. Bogaerts, R. Gijbels, W.J. Goedheer, Anal. Chem. 68 (1996) 2296.
6 A. Bogaerts, R. Gijbels, Anal. Chem. 68 (1996) 2676.
7 A. Bogaerts, R. Gijbels, J. Vlcek, J. Appl. Phys. 84 (1998) 121.
8 A. Bogaerts, R. Gijbels, R.J. Carman, Spectrochim. Acta Part B 53 (1998) 1679.
9 A. Bogaerts, R. Gijbels, J. Appl. Phys. 86 (1999) 4124.
10 A. Bogaerts, M. Yan, R. Gijbels, W.J. Goedheer, J. Appl. Phys. 86 (1999) 2990.
11 A. Bogaerts, R. Gijbels, IEEE Trans. Plasma Sci. 27 (1999) 1406.
12 A. Bogaerts, R. Gijbels, W.J. Goedheer, Spectrochim. Acta Part B 54 (1999) 1335.
13 A. Bogaerts, R. Gijbels, Behavior of the sputtered copper atoms, ions and excited species in a radio-frequency and direct current glow discharge, Spectrochim. Acta Part B 55 (2000) 279.
14 J. Vlcek, J. Phys. D 22 (1989) 623.
15 A. Bogaerts, R. Gijbels, Spectrochim. Acta Part B 53 (1998) 437.
16 V. Hoffmann, private communication.
17 F. Guimaraes, J. Bretagne, Plasma Sources Sci. Technol. 2 (1993) 127.
18 C.M. Ferreira, J. Loureiro, A. Ricard, J. Appl. Phys. 57 (1984) 82.
19 A. Bogaerts, R. Gijbels, J. Vlcek, Spectrochim. Acta Part B 53 (1998) 1517.